Supplementary material for

Formation and properties of spindle-shaped aragonite mesocrystals from Mg-bearing solutions

Zsombor Molnár[1,2], Péter Pekker[1], Aleksander Rečnik[3], Mihály Pósfai[1,2]

[1] University of Pannonia, Research Institute of Biomolecular and Chemical Engineering, Nanolab, Hungary, 8200, Veszprém, Egyetem st. 10.

[2]HUN-REN–PE Environmental Mineralogy Research Group, Hungary, 8200, Veszprém, Egyetem st. 10.

[3]Jožef Stefan Institute, Department of Nanostructured Materials, Slovenia, 1000, Ljubljana Jamova cesta 39.

Measured titration curves

In our titration experiments we used a similar technical approach as reported by Gebauer et al. (2008), in order to follow the nucleation of $CaCO_3$ phases and for sampling the solutions around the point of nucleation for the analysis of the precipitated solids. Fig. S1 shows the averaged titration curves from our experiments with different solution compositions (at increasing dissolved Mg:Ca ratios). We calculated the derivatives of the averaged titration curves in order to define accurately the point of nucleation. Using the volume ratios of the buffer and titrant solutions and the known ionic compositions of the solutions at the point of nucleation we calculated the ionic strength and saturation indices (SI). We used the $\log(K_{sp})$ values with respect to the different solid phases reported by Plummer and Busenberg (1982)[1] for calcite, aragonite and dolomite; Brečević and Nielsen (1989)[2] and Gebauer et al. (2008)[3] for pure ACC, and Purgstaller et al. (2019)[4] for Mg-bearing ACC (assuming 50% Mg content in the amorphous phase).

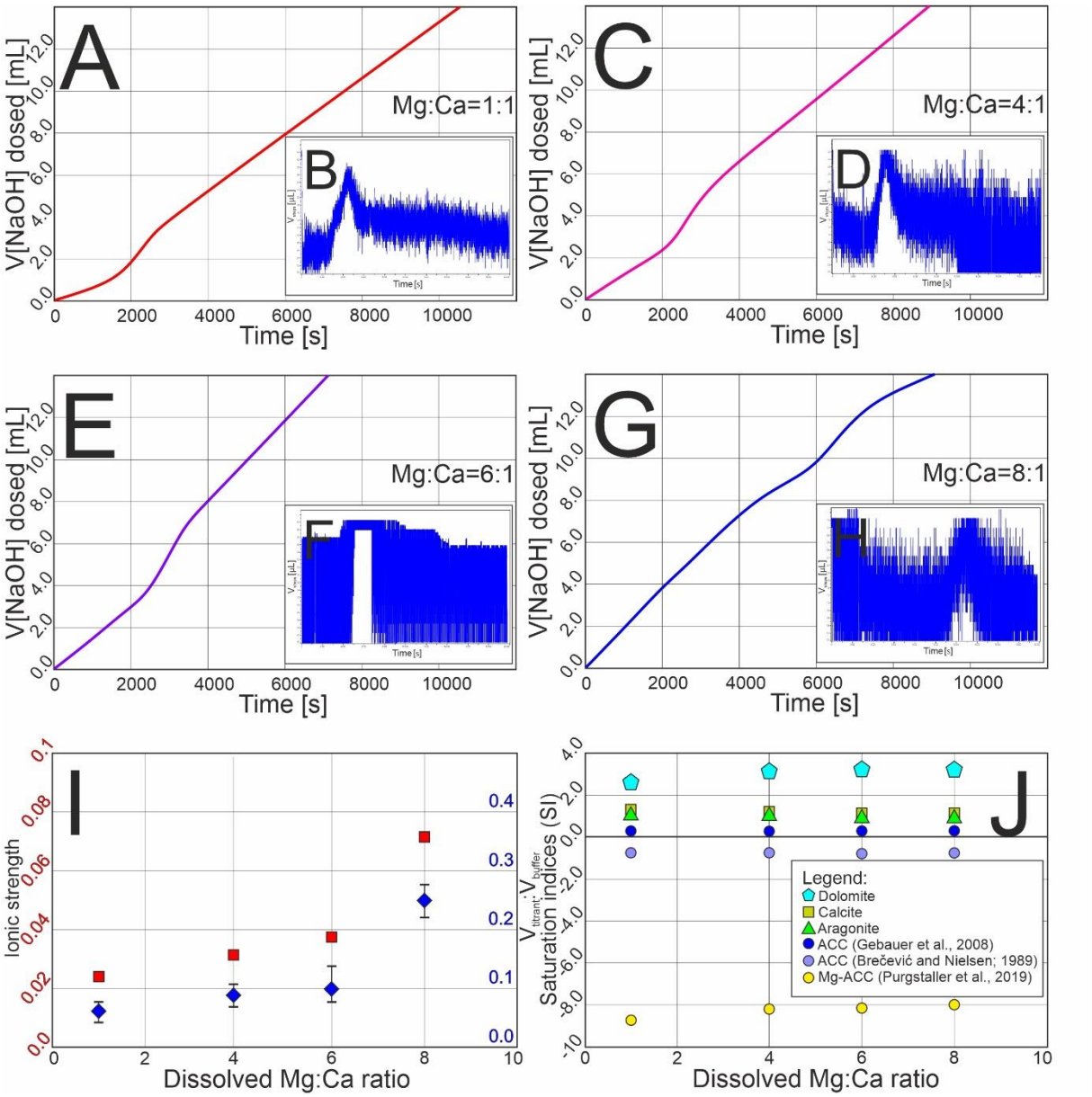

Fig. S1 – **(A) – (H)** Averaged titration curves and their derivatives (inserts in the lower right) for solutions with different Mg:Ca ratios. **(I)** Volume ratios of the buffer and dosed titrant solutions (blue) at the point of nucleation and the corresponding values for calculated ionic strength (red). **(J)** Calculated saturation indices (SI) of calcite, aragonite, dolomite and Mg-bearing ACC (assuming 50 mol% $MgCO_3$ content) at the point of nucleation.

Analysis of the co-occurrence of Mg-ACC and aragonite

We observed the co-occurrence of globular amorphous particles and spindle-shaped aragonite aggregates, representing the first stages of amorphous to crystalline transformations (Fig. S2). HRTEM images and their FFT patterns did not show any lattice fringes (Fig. S2B) and discrete reflections (Fig. S2C), respectively; thus, we interpreted them as amorphous phases. In contrast, the elongated aggregates showed periodic spacings with sharp maxima in the FFT (Fig. S2E-F). Based on the measured d-values we identified the aggregates as aragonite (*Pmcn* space group) (Fig. S2). The amorphous particles appeared even on the tips and the sides of the spindles (Fig. S3A-B). The amorphous particles have significant Mg content (Fig. S3C-D); however, it was difficult to measure the exact Mg/Ca ratio due to the tight association of amorphous and crystalline materials. SAED patterns showed diffuse rings and discrete intensity maxima (Fig. S3E), and the calculated radial intensity function also revealed the superposition of discrete peaks onto a broad feature caused by amorphous material. The calculated *d*-values of the amorphous peak indicate the presence of Mg-bearing amorphous calcium carbonate and the discrete peaks correspond to aragonite (Fig. S3F).

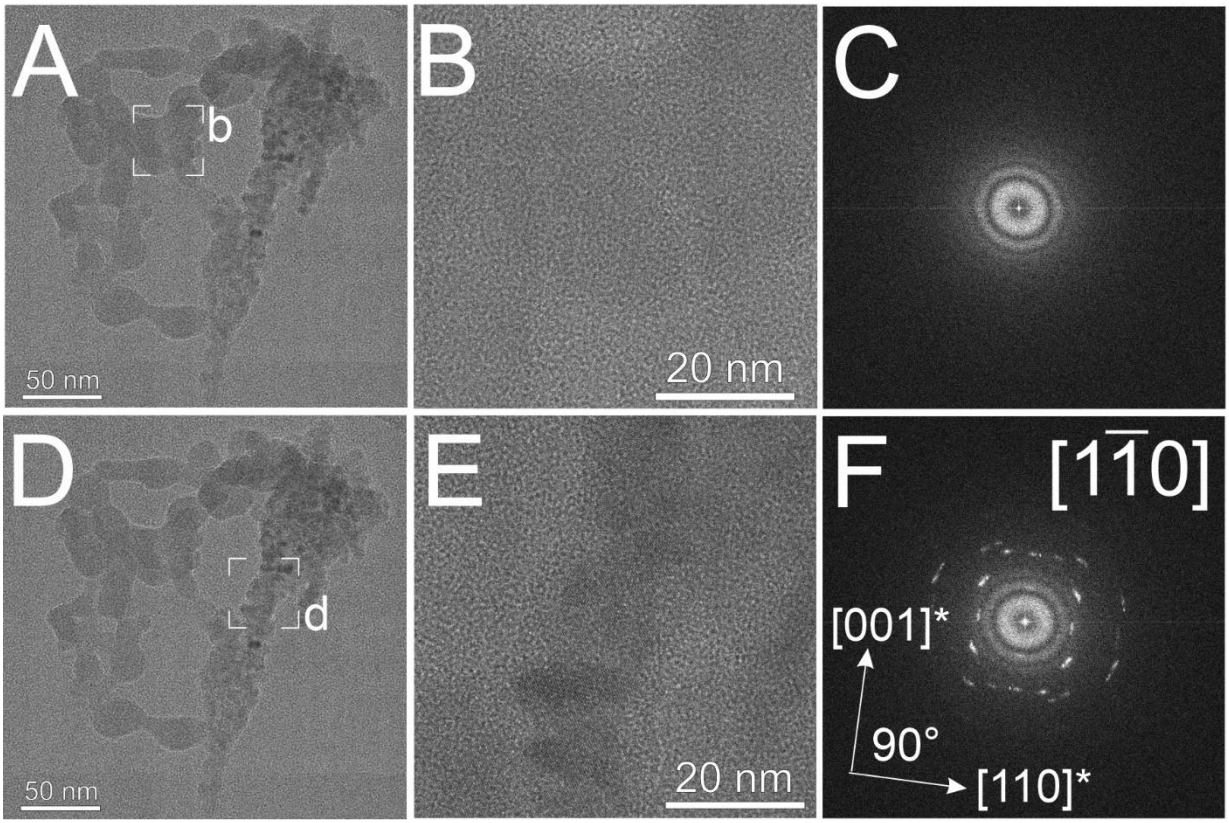

Fig. S2 – TEM analysis of co-occurring amorphous and crystalline carbonate phases. **(A)** and **(D)** TEM BF image of Mg-ACC – aragonite aggregates presented in Fig. 2 in the main article, with the positions of the HRTEM images and FFTs marked. **(B)** HRTEM image and **(C)** calculated FFT of the amorphous part. The lack of lattice fringes in (B) and the absence of diffraction maxima in (D) indicate that the few-tens-of-nm-large globular particles were amorphous. (E) HRTEM image and (F) calculated FFT of the crystalline part, with the measured d-values and angles confirming it is aragonite. The FFTs were calculated from the entire areas of panels (B) and (E).

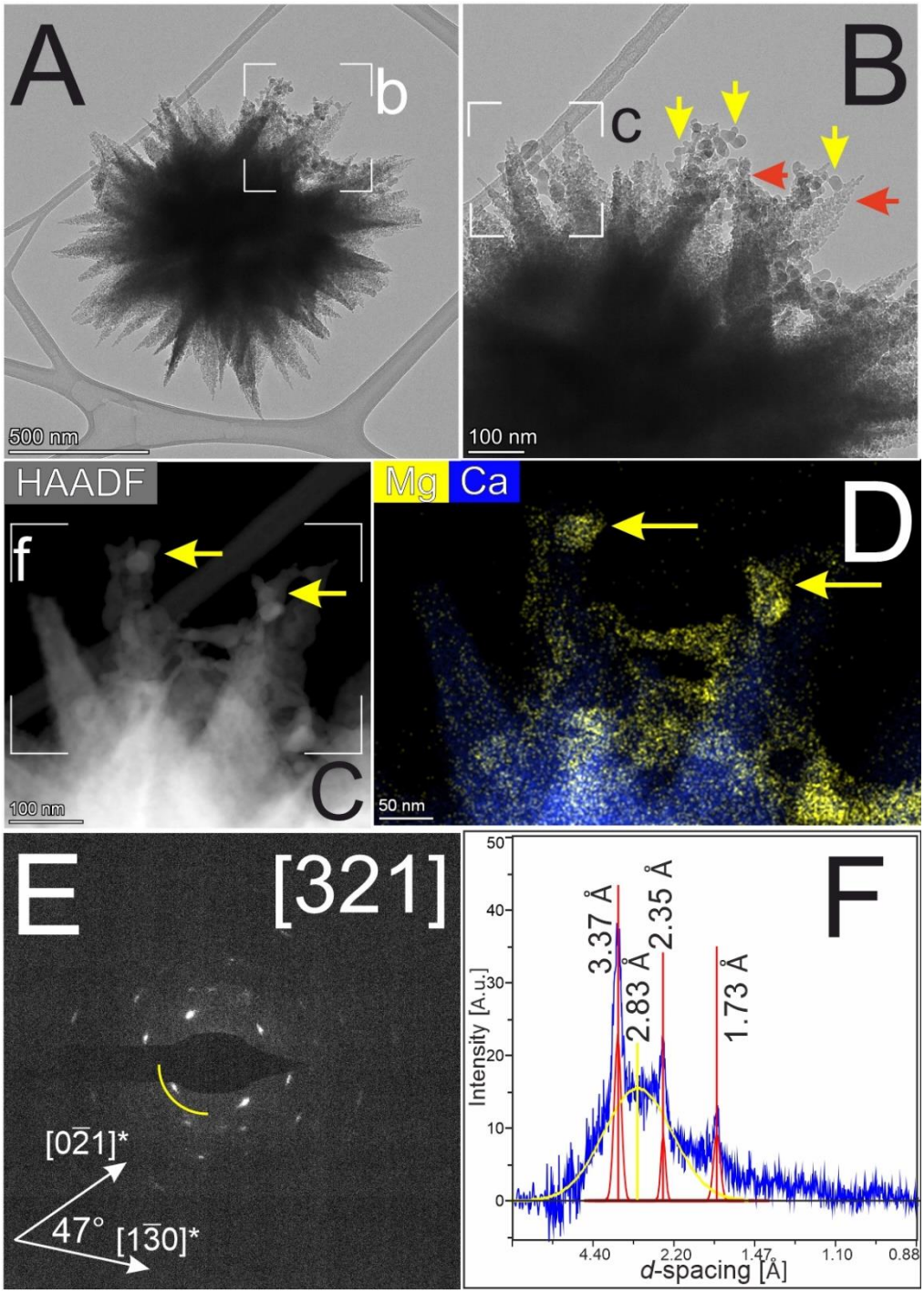

Fig. S3. – Co-occurrence of amorphous globules and aragonite spindles. **(A)** and **(B)** BF TEM images show the random occurrence of globular particles (yellow arrows) on the aragonite spindles (red arrow). **(C)** STEM HAADF image and **(D)** corresponding STEM EDX elemental maps reveal that the globules have significant Mg content. **(E)** SAED pattern and **(F)** a radial intensity distribution calculated from it show the superposition of discrete peaks of aragonite (marked by red in **F**) onto a broad amorphous background peak (yellow). The center of the peak produced by amorphous material is around 2.8 Å, indicating the presence of Mg-bearing ACC.

HRTEM analysis of the structure of aragonite spindles

We performed a detailed TEM analysis of the structure and the crystallographic coherence of nanocrystals within aragonite spindles, focusing on an 'arm' of an intergrown spindle (Fig. S4A-B). HRTEM images (Fig. S4C and E) and their FFT patterns (Fig. S4D and F) show that there is only a slight misorientation between the distinct parts of the arms, producing a 3°–5° difference between the [001] directions. We also observed doubled periodicity along the [110]* direction which could imply the presence of twinning between aragonite nanocrystals.

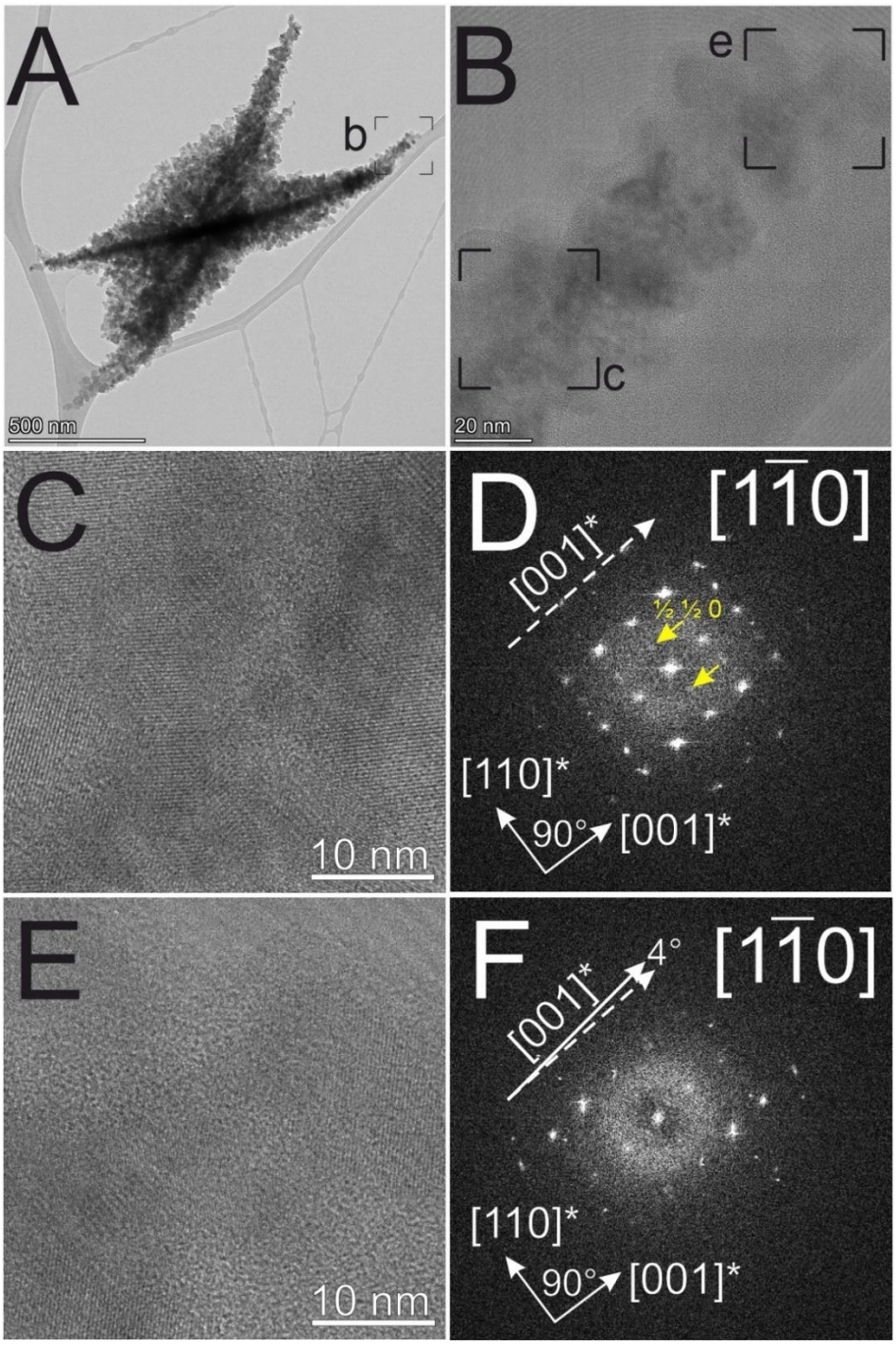

Fig. S4. – Structural analysis of an individual aragonite spindle. **(A)** and **(B)** BF TEM images highlight the studied areas. (**C** and **E**) HRTEM images and (**D** and **F**) corresponding FFTs show that only a slight misorientation occurs between the [001] directions (white dashed lines) of neighboring nanocrystals of the spindles. The FFT also revealed doubled periodicity along the [110] direction (yellow arrows) which could be caused by twinning between aragonite nanocrystals.

Electron tomographic measurements of aragonite spindles

In order to study the morphological properties of intergrown aragonite spindles we performed tomographic measurements in STEM mode. The STEM tomography analysis revealed that the star-like grains consisting of intergrown spindles have complex morphologies (Fig. S5; S6 mov. 1-2). The angle between the longest axes of the intergrown spindles (i.e., their [001] crystallographic directions) is typically around 99° (± 2°) (Fig. S5B). Even though this specific angle suggests a structurally determined orientation relationship, we could not confirm a twin relationship between the intergrown aragonite spindles. The tomographic measurements also confirm the presence of holes of various sizes (up to tens of nm) within the aragonite aggregates, located in random positions (Fig. S5C; S6-mov. 3).

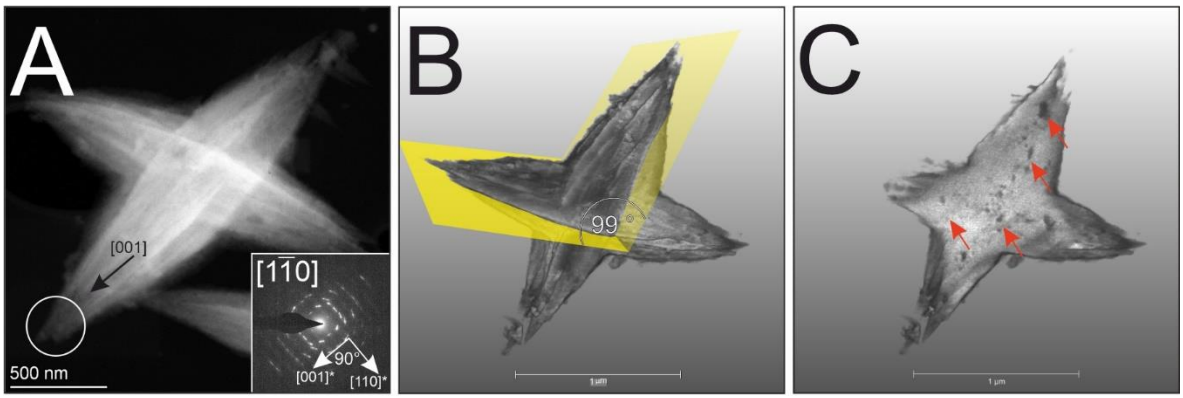

Fig. S5. – Morphological aspects of intergrown aragonite spindles. **(A)** STEM HAADF image of an aragonite grain with the corresponding SAED pattern (obtained from the area marked by the white circle). **(B)** STEM tomographic reconstruction showing that the angle between the longest axes of the spindles is around 99° (± 2°), suggesting an incidental intergrowth of the spindles. **(C)** The measurements also confirm the presence of few-nm-large holes within the spindles (red arrows).

Mov. S6_1 – Reconstructed surface model of intergrown aragonite spindles, based on a dataset obtained using STEM-HAADF electron tomography.

Mov. S6_2 – Reconstructed volume model of intergrown aragonite spindles, based on a dataset obtained using STEM-HAADF electron tomography. Less dense, translucent material surrounding the spindle-shaped particles probably represents Mg-ACC.

Mov. S6_3 – Orthoslice image series through aragonite spindles, showing up to tens-of-nm-large holes among the aragonite nanocrystals.

Aging the precipitated aragonite spindles

After the synthesis of aragonite spindles, we studied the structural and textural evolution of the formed aragonite spindles by aging them in their mother solution for two months. Then we filtered the solution with a vacuum filter, as was detailed in the Materials and methods section of the main text. After two months of aging, we found aggregates of few-µm-large, lath-shaped aragonite single crystals (Fig. S7A). HRTEM images did not show any remnants of the granular texture of aragonite, which was typical for the spindle-shaped aggregates, the laths were perfect single crystals (Fig. S7B). Nevertheless, the doubled periodicity along the [110]* direction was typically observed (Fig. S7C).

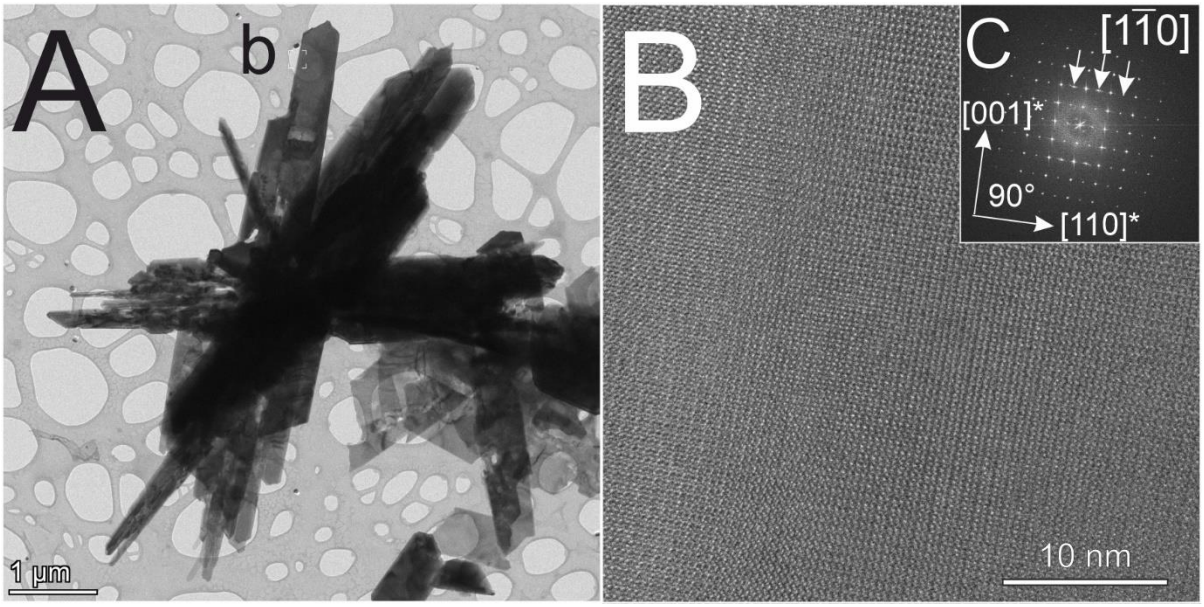

Fig. S7 – Aragonite spindles transformed into lath-shaped crystals after two months of aging. (**A**) TEM BF image of aggregates of lath-shaped aragonite crystals. **(B)** HRTEM image with **(C)** a corresponding FFT did not show any remnants of the previous granular texture of aragonite spindles, the particles were prefect single crystals. FFT patterns typically show doubled periodicity (white arrows) along the [110]* directions.

References:

1. L. N. Plummer, E. Busenberg, *Geochim. Cosmochim. Acta*, 1982, **46(6),** 1011-1040.
2. L. Brečević, A. E. Nielsen, *J. Cryst. Growth*, 1989, **98 (3),** 504-510.
3. D. Gebauer, A. Volkel, H. Cölfen, *Science,* 2008, **322 (5909)**, 1819–1822.
4. B. Purgstaller, K. E. Goetschl, V. Mavromatis, M. Dietzel, *CrystEngComm*, 2019, **21**, 155-164.